Histochem Cell Biol (1997) 107:267–278

ORIGINAL PAPER

Shuqing Liu · Donald L. Weaver · Douglas J. Taatjes

Three-dimensional reconstruction by confocal laser scanning microscopy in routine pathologic specimens of benign and malignant lesions of the human breast

Accepted: 7 November 1996

Abstract Confocal laser scanning microscopy (CLSM) has become an exciting new instrument because of its increased resolution over conventional wide-field microscopy and its high performance three-dimensional (3D) optical sectioning. Although CLSM has been used extensively in cell biology, few applications have been reported in routine clinical pathology. In this study, 3D reconstruction was performed on routine formalin-fixed, paraffin-embedded tissues of normal mammary duct, simple ductal hyperplasia, intraductal papillary hyperplasia, ductal carcinoma in situ, invasive carcinoma, and lymph node metastatic carcinomas of the human breast by using computer-assisted CLSM in conjunction with a 3D reconstruction software package (microVoxel). The selected specimens were sectioned at 30 μm, mounted on glass slides, and stained with the DNA fluorescent probe, YOYO-1 iodide. The nuclear DNA and chromatin texture were clearly demonstrated after pretreatment with RNAase and hydrolysis with 2 N HCl. High quality 3D images were obtained by processing the optical section stacks with volume render and surface display parameters in microVoxel. 3D morphologic characteristics of different breast lesions were examined in various orientations by angular image rotation. The clearly benign lesions (simple ductal hyperplasia and intraductal papillary hyperplasia) revealed similar 3D morphologic features, including: (1) smooth nuclear surface and homogeneous chromatin fluorescence intensity; (2) hyperplastic cell nuclei showing similar shape and volume; and (3) clear-cut margin of basement membrane defined by spindle-shaped myocytes of the ductal outer layer. In contrast, carcinomas displayed remarkably different features in 3D morphology, including: (1) irregular nuclear surface; (2) marked nuclear pleomorphism (irregular, angulated and indented shape of nuclear volume); (3) irregular and coarse chromatin texture; (4) chaotic arrangement of tumor cell nuclei; and (5) absence of myocytes, indicating no clear margin at the site of infiltration of cancer cells. In conclusion, nuclear structure, specifically demonstrated by CLSM of YOYO-1 iodide fluorescently stained cells, used in tandem with 3D volume morphologic reconstruction, may provide a useful research diagnostic tool in pathology.

S. Liu[1] · D. L. Weaver · D. J. Taatjes (✉)
Department of Pathology, Cell Imaging Facility,
Medical Alumni Building, University of Vermont, Burlington,
VT 05405, USA
Tel. +1–802–656–0373; Fax +1–802–656–8892
e-mail: dtaatjes@salus.uvm.edu

[1] *Present address:* Research Division, Evanston Hospital,
2650 Redge Avenue, Evanston IL 60201, USA

Introduction

Three-dimensional (3D) visualization of pathologic specimens has long been a dream of pathologists. Conventional light microscopically reconstructed structures of a given lesion require mechanical sectioning which often damages the specimen and produces sections without mutual alignment. Moreover, these methods are time consuming and laborious. In addition, conventional light microscopic methods are difficult or impossible to apply to thick specimens because the superimposition of out-of-focus structures degrades image contrast and resolution (Sasano et al. 1993). However, high quality 3D images may be helpful, or even essential, in arriving at a definitive diagnosis, especially for borderline lesions or tumors (Tekola et al. 1994a; Chen et al. 1995).

Confocal laser scanning microscopy (CLSM) allows the acquisition of optical sections from a thick specimen and has become an exciting new instrument in biomedical research because of its increased resolution over conventional wide-field light microscopy and its utility for subsequent 3D reconstruction analysis. It can provide a thinner, in-focus plane with better quality 2D digital images, while out-of focus blur can be reduced considerably. Thus, much sharper and clearer images can be obtained (Tekola et al. 1994a). In this way, intra- and/or inter-cellular stereo structures can be visualized clearly, and hidden diagnostic features of malignancy (rare event) can be revealed. For instance, nuclei with angu-

lated and irregular shape and a coarse chromatin pattern hidden in the thick specimen of borderline lesions can be detected by scrolling through different levels of serial optical sections. This is critical in differentiating malignancy from benign or borderline lesions. Furthermore, a 3D reconstructed image of the specimen can be rotated and animated at any angle, so that a particular lesion or nucleus can be emphasized by a variety of 3D reconstruction techniques, which is impossible with conventional wide-field light microscopy.

CLSM has been used extensively in cell biology (Shuman et al. 1989; Chen et al. 1995). The high resolution and variety of visualization parameters, together with its high performance, non-invasive optical sectioning, makes CLSM extremely useful for studying the 3D morphology of biologic structures (Brakenhoff et al. 1985). Although some applications have been reported in experimental pathology (Boon et al. 1993; Sasano et al. 1993; Tekola et al. 1994a; King et al. 1995), comprehensive CLSM application on human diagnostic materials in routine pathology has only been reported in the studies of Boon and co-workers on human cervical smears of routine cytology (Boon et al. 1993, 1994, 1995) and of King and co-workers on a case of borderline papillary serous tumor of the peritoneum (King et al. 1995).

In this study, 3D reconstruction was performed on routine formalin-fixed, paraffin-embedded tissues of benign (normal, simple hyperplastic, and papillary hyperplastic) and malignant (carcinoma in situ, invasive, and lymph node metastatic) tissues of the human breast by using computer-assisted CLSM together with 3D reconstruction. The goals of our study were threefold: (1) to attempt to demonstrate the usefulness of CLSM in routinely obtained surgical pathology tissue; (2) to demonstrate the 3D morphologic characteristics of different entities of the human breast; and (3) to present 3D morphologic correlates for benign and malignant specimens of the human breast.

Materials and methods

Specimens and staining

Sixteen cases, including normal mammary ducts and lobules, ductal simple and papillary hyperplasia, ductal carcinoma in situ, ductal invasive and lymph node metastatic carcinomas were selected from routine clinical specimens collected in the Surgical Pathology suite at Fletcher Allen Health Care from 1991 to 1996. From the 10%-buffered formalin-fixed, paraffin-embedded tissues, serial sections were cut at 5 μm and 30 μm. The 5-μm slices were stained with hematoxylin and eosin for conventional wide-field light microscopic observation. The 30-μm-thick sections were stained with the DNA fluorescent probe, YOYO-1 iodide (Tekola et al. 1994b), as follows. The sections were deparaffinized with xylene (2×10 min) and rehydrated with 100%, 95%, and 70% alcohol (2×5 min) and rinsed in distilled water for 2 min. The specimens were then fixed with 10% neutral buffered formalin for 30 min and washed with tap water. After rinsing with distilled water and 0.01 M phosphate buffer, 0.15 M NaCl, pH 7.2 (PBS), nuclear RNA was removed by incubating the sections for 30 min at 37°C in 200 μl of ribonuclease A (RNAase; Sigma, St. Louis, Mo., USA) at a concentration of 160 mg/ml in PBS. Next, DNA was hydrolyzed with 2 N HCl for 25 min at 27.5°C. After rinsing with distilled water for 2 min, the sections were covered with 200 μl of YOYO-1 iodide (Molecular Probes, Eugene, Ore., USA) diluted 1:2000 in one-fifth strength PBS. The PBS was diluted 1:5 with distilled water to reduce the salt concentration, since higher salt concentration has been shown to reduce the fluorescence intensity of YOYO-1 iodide (Tekola et al. 1994b). To this 200 μl working solution of YOYO-1 iodide, 20 μl of 0.1 N HCl was added and the final solution was stored in the dark at 4°C until use. Homogeneous fluorescence intensity of nuclei at different depths of the confocal slices was obtained by performing the YOYO-1 iodide incubation for 1 h with agitation in the dark. Afterwards, the sections were rinsed with distilled water, dehydrated with 70%, 95%, and 100% alcohol (2×3 min), xylene (2×5 min), and finally covered with Vectashield anti-fade mounting media (Vector Laboratories, Burlingame, Calif., USA) and a glass cover slip (no. 1), then sealed with finger nail polish. Sections were stored at 4°C in the dark until CSLM examination.

Confocal microscopy and optical sectioning

Confocal optical sectioning was performed with a BioRad (Hercules, Calif., USA) MRC 1000 confocal scanning laser system mounted on an Olympus BX50 upright microscope. Confocal optical sectioning on the representative fields of different entities of the human breast was performed with the confocal laser scanning microscope as follows: A krypton/argon laser with an excitation wavelength of 488 nm operating at an intensity of 3% of maximum was used to activate the green fluorescence of the YOYO-1 iodide-stained nuclear DNA. A confocal iris aperture of 0.7 mm (smallest allowable on the MRC 1000) and a gain setting of 720–960 v were chosen to achieve maximum image sharpness and contrast. Optical sections were collected throughout the entire stained thickness of the paraffin sections with a Z-step interval of 0.3 μm or 0.6 μm. To minimize fluorescence bleaching during scanning, low laser light source intensity was applied. To maximize the 3D visualization of the sections, 45–96 planes of optical sections were collected for each representative field of different entities of the breast. The clearest images were obtained by using an average Kalman filtering of 7 times. High magnification images were obtained with a 60× planapo objective lens (NA=1.4, oil immersion) and a software zoom factor of 2.6× for all the optical sectioning. Use of identical image parameters permitted easy comparison for further two-dimensional (2D) and 3D image analysis. The size of each 2D image with 256 gray levels was 768×512 pixels times 8 bits, requiring 23.2 Mbytes of hard disk space for digital storage of a set of 60 serial 2D optical images. The collected digital images were transferred to high capacity (1 Gbyte) optical disks for archival storage, and imported into the microVoxel 3D reconstruction software program (Indec Systems, Mountain View, Calif., USA). Imported files in BioRad.*PIC* format (dimension of 768×512×53, size of 0.37×0.37×0.60 μm) were converted to the microVoxel.*IMG* format (dimension of 512×512×53, size of 1.04×0.69×0.50 μm). The 3D image processing was performed on a Gateway 2000 P5-60 computer. The collected confocal optical sections and the 3D reconstructed images were printed with a Mitsubishi color video dye-sublimation copy processor.

Image analysis

Preprocessing and enhancement of digital images

Digital microscopic images contain high frequency noise due to statistical counting errors that occur during the imaging process (Chen et al. 1995; Shotton 1995). Deblurred 3D images obtained with a confocal laser scanning microscope often contain structures that are represented by only a small portion of the dynamic range of the image display system. When this type of image is displayed without enhancement, the data of interest will be translated into only a few intensity levels in the display, suppressing desired details in the resultant image (Chen et al. 1995). Image enhancement

is necessary for realistic visualization and analysis. To improve the clarity of image presentation, digital image enhancement was performed before processing for 3D reconstruction as follows:

1. Contrast stretch. This command rescales the active display box so that the dimmest pixels are set to intensity 0 and the brightest to intensity 255. The resulting image takes maximum advantage of the display contrast.
2. Edge enhancement. This technique allows the selection of a crisping convolution. For most of the digital images collected in this study, C5A or C7A was used. These are high-pass filters, which accentuate local (i.e., high frequency) structural features and de-emphasize global (low frequency) ones, making the image look sharper.
3. Smoothing. This is a low-pass filter, which de-emphasizes local structural features and accentuates global ones. The resulting images look slightly blurred (softened), but with reduced noise. For most of the images, the filter S5A or S7A was selected in this study.
4. Median filter. In median filtering, the pixels in the window are ranked, and the middle value, e.g., the fifth, is placed in the center pixel. The window is moved over the image as in a convolution. This technique was particularly effective for removing random noise from an image while retaining small features. The size of the filter window we used in this study was a 3×3 matrix.
5. Local contrast enhancement (LCE). LCE accentuates the edges in the image, which was particularly useful for clarifying the boundary of the nuclei and sharpening the structure of the breast tissues. LCE is similar to the global operation contrast stretching. A selected window was moved over the image, and the range of pixel values within the window was calculated, then the deviation of each pixel from the mean was multiplied by the expansion factor. The window was then advanced by its entire width, not one pixel at a time. We used a window size of 5 pixels, with an expansion factor of 3.00 for all of the images.

Digital image processing

As briefly described above, the Z-series of 3D digital images was projected on the monitor in a given direction of space, thus producing a 2D image for visualization. Although this projection appears at first sight as an oversimplification of all the information (since no volume is retained), this method is nevertheless very useful in understanding 3D data sets because it can be combined with tools to help the observer to understand this 3D information (Lucas et al. 1996). To create realistic 3D digital images, microVoxel (version 2.2, 32 bit) software was used. The first step in the process of analyzing volume image data with microVoxel is to convert the BioRad.*PIC* image files collected from the confocal laser scanning microscope into a form that microVoxel is able to interpret. Our version of microVoxel restricts volumes to a maximum of 512 units on a side. Thus, a volume, for example, which collected from the confocal laser scanning microscope was 768×512×90 needed to be resized to no greater than 512×512×90. This was easily accomplished by the software for file conversion provided in the microVoxel package.

To achieve accurate visualizations of the true relative dimensions of a volume from microVoxel, both the size and normalization values needed to be set correctly. Since our goals were to recreate realistic 3D digital images from the paraffin-embedded, YOYO-1 iodide-stained tissues of the breast, and for a volume reconstruction to appear the same as its natural physical shape of volume and intercorrelation, we also needed to set screen normalization values such that the ratio between these values is the same as those of microVoxel's physical dimensions. To create realistic 3D digital images from the paraffin-embedded tissues, correction of anisotropic voxels resulting from the flattening of the coverslip needed to be performed. The correction, or rescaling factor, for screen normalization in our data sets was 1.10 for the *y* axis and 3.50 for the *z* axis.

MicroVoxel provides a variety of tools for 3D reconstruction. The main functions pertaining to 3D digital image processing and reconstruction we found particularly useful were morphology filters and LCE before the 3D rendering. Prior to generating a shaded surface display (SSD), appropriate thresholding was essential to insure that the nuclei were well separated and displayed a realistic 3D surface appearance.

Morphology. Gray scale morphologic filtering is a useful image processing tool for improving the connectivity or boundary information of the volume data. Since our volume data were gathered one slice at a time, data in one slice may be statistically independent from that in other slices, which makes it appropriate to morphologically filter each slice independently. Since the information was correlated in the breast tissues in all three dimensions, a dilation operation 3D morphologic filter was used for all of the digital image data. The depth and neighbor, as well as the number of morphological filter iterations applied to the volume was one. Subsequently, each examined voxel, with the maximum number of its neighboring voxels as defined by the geometric structuring element, was replaced.

LCE. LCE is a specialized image processing tool that is very helpful in several of the most common image problems. By employing the LCE filter, and carefully adjusting the contrast and mean lookup table, background noise was removed and edges were enhanced. The size of the convolution kernel (contrast/mean kernel) we used for our digital image data was 3×3×1.

Conventional wide-field fluorescence microscopy

YOYO-1 iodide-stained 30-µm-thick paraffin-embedded sections were viewed with an Olympus BX50 upright light microscope. Fluorescence signal was observed using a blue excitation filter cube (U-MWIBA: wide band interference filter blue excitation with bandpass barrier, exciter filter BP 460–490 nm, dichromatic beamsplitter DM 500 nm, and bandpass barrier filter BA 515–550 nm). Digital images (640×480 pixels) were collected with a Sony DXC-960MD/LLP CCD camera connected via an RS-170 cable to a video frame grabber on a Sun SPARCstation 5. The digital images were imported into Paint Shop Pro (JASC, Minnetonka, Minn., USA) and printed with a Mitsubishi dye-sublimation printer.

Results

Improved resolution of 2D digital images by CLSM: optical sectioning on different entities of the human breast

Images with obscured detail were obtained by using conventional wide-field fluorescence microscopy from the 30-µm-thick sections of the breast. Virtually no details of nuclear structure could be revealed due to the inherent fluorescence haze associated with structures located above or below the focal plane (not shown).

In contrast, much improved 2D digital images with better resolution were obtained from various entities of the human breast by using optical sectioning with the confocal laser scanning microscope. Figures 1–6 show examples of the projection of Z-series of 2D digital image stacks taken from normal tissue (Fig. 1A, B), simple ductal hyperplasia (Fig. 2A, B), intraductal papillary hyperplasia (Fig. 3A, B), fibroadenoma (Fig. 4A, B), carcinoma in situ (Fig. 5A, B), and ductal invasive carcinoma (Fig. 6A, B). For details of the different lesions, see the legends to the figures.

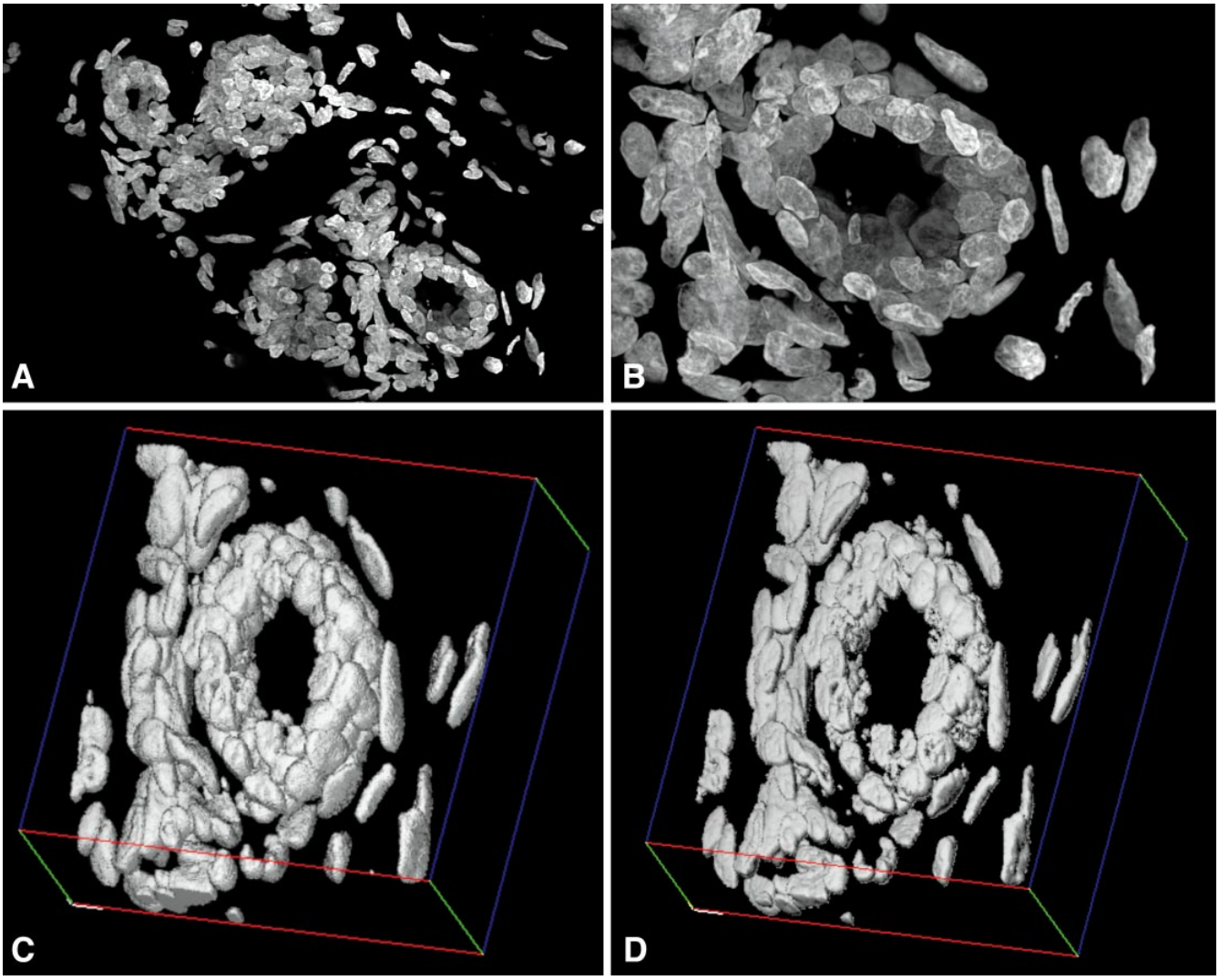

Fig. 1 **A** Digital image of Z-series (planes 1–46) of optically sectioned 30-µm-thick formalin-fixed, paraffin-embedded, YOYO-1 iodide-stained section of a normal human mammary duct by confocal laser scanning microscopy (CLSM) with a Z-step interval of 0.6 µm using a 60× objective lens. **B** High power of Z-series of two-dimensional (2D) images of the normal mammary duct shown in **A**. Ductal epithelial cells with similar shape and size as well as homogeneous intensity of YOYO-1 iodide fluorescence are arranged in a single layer, surrounded by spindle-shaped myocytes (60× objective, NA 1.4, zoom factor 2.6, Z-step interval 0.3 µm). **C** Three-dimensional (3D) view of shaded surface display of the same duct shown in **B**. The nuclear surface appears smooth with homogeneous fluorescence intensity. The 3D volume was rotated at –21° on both the *x* and *y* axes and –7° on the *z* axis. **D** 3D view of volume render of the same duct shown in **B**, rendered under the First Voxel mode. The nuclei are singly layered with homogeneous fluorescence intensity and similar round or ovoid shapes. The rotation angle of the volume is the same as for **C**

3D rendering and reconstruction

Two different techniques were applied for 3D reconstruction of image stacks: shaded surface display and volume rendering.

Shaded surface display (SSD)

SSD is most effective in demonstrating the structure of the nuclear surface. Creating an SSD object was a time-consuming task with some of the larger data sets. However, having a well-defined somewhat “smooth surface” was important for generating quality results for SSD objects. The object could be rotated, translated, colored, and highlighted. A given 3D digital volume data set collected from different entities of the breast has several independent complex structural interactions, even within a nucleus with different biological functions. The ability to extract each one of these diagnostic features and treat it as a separate entity is desirable. However, the process of defining an object with a volume is not trivial, requiring much interaction from the investigator.

Unfortunately, in some of the raw slice data sets, the outer edge data of the object of interest has roughness or noise associated with it, causing the SSD to appear to have a rougher looking surface than may be desired. Some image processing of the original data set can help to remove this surface roughness effect. Thresholding is the first important parameter to define or extract an ob-

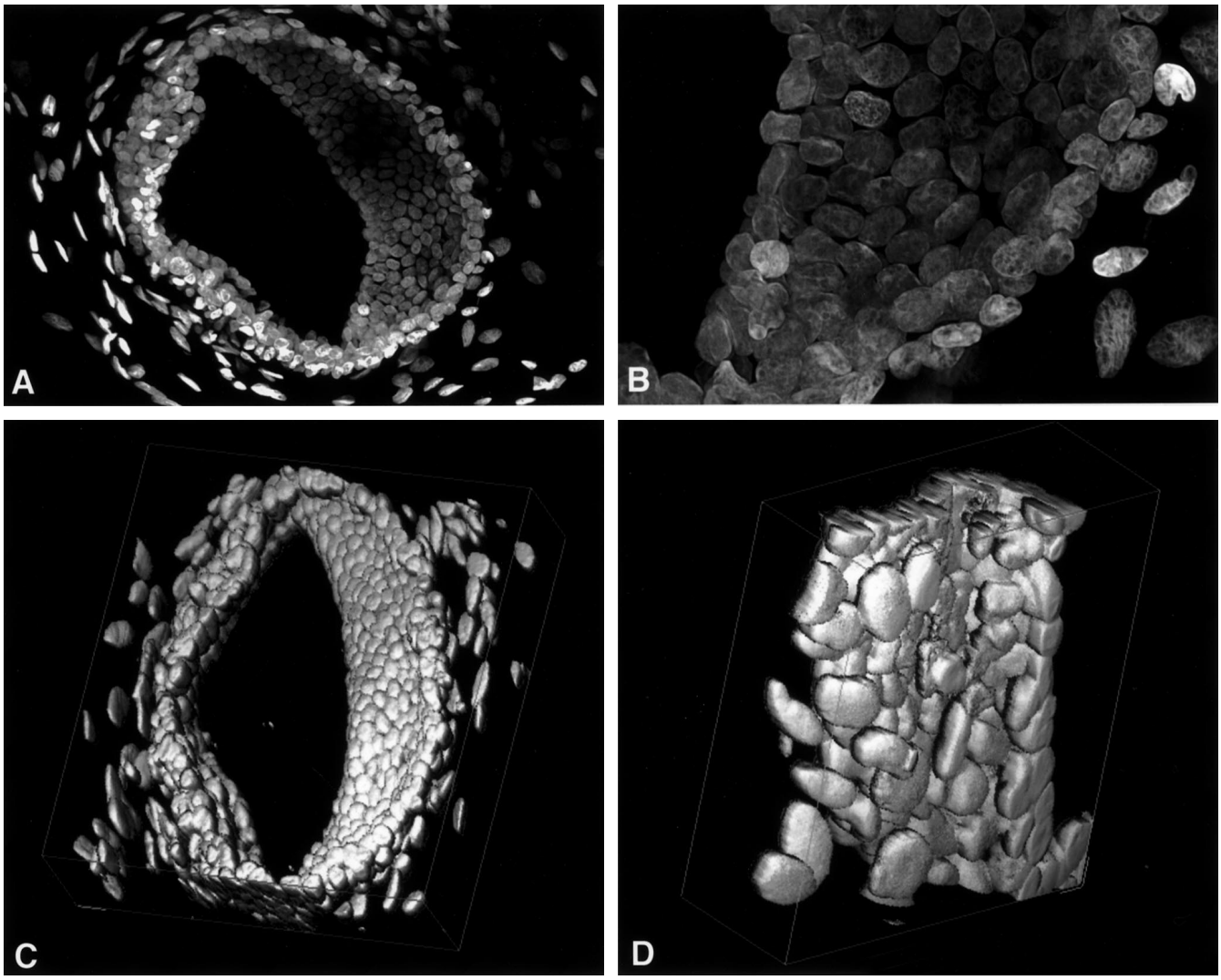

Fig. 2 **A** Digital image projection of a Z-series of 36 optical sections taken by CLSM from a 30-μm-thick section of a mammary duct with simple hyperplasia. Multilayered nuclei surrounded by spindle-shaped myocytes display similar shape and size, as well as homogeneity of fluorescence intensity (Z-step interval 0.6 μm, 60× objective). **B** Higher power digital image of the same hyperplastic duct shown in **A**. Subtle nuclear chromatin texture is shown by the homogeneous intensity of YOYO-1 iodide fluorescence. One or two small nucleoli were occasionally seen, and the nuclear rim is very thin. The spatial correlation between nuclei, and the size and shape of nuclei are regular and similar (Z-projection of 56 digital image planes with Z-step interval of 0.3 μm, 60× objective, zoom factor 2.6×). **C** 3D view of volume render of the same duct shown in **A** rendered with the First Voxel mode. Rotation angle was –21° on both the *x* and *y* axes, and –7° on the *z* axis. **D** High power 3D view of volume render of the same field shown in **B**, rendered with the First Voxel mode. The nuclei are round with smooth surfaces, and display homogeneous fluorescence intensity. Rotation angle was –138° on the *y* axis, –37° on the *x* axis, and 0° on the *z* axis

ject. By defining the minimum and maximum intensity values to be included in the definition of an object, each slice displayed has an image of the original intensity value and binary image of the slice showing what is included (bright) and what is excluded (dark) from the volume. To achieve satisfactory 3D SSD images, the following parameter settings were chosen in this study: image size, 512; Z-clip, 512; image scale, 65%; depth weight, 30%; Interaction, absolute; edge size, 1; color setting: red, green and blue were set at 68% to obtain the best contrast and clarity. The rotation angle and light position were adjusted according to preferences for effect and the goals in analyzing a given image. 3D reconstructions rendered via SSD are shown in Fig. 1C (normal mammary duct), Fig. 3C, D (intraductal papillary hyperplasia), Fig. 4C, D (fibroadenoma of the breast), Fig. 5E (ductal carcinoma in situ), and Fig. 6C, D (ductal invasive carcinoma).

Volume render

This provides the most revealing look at internal and external structures in the digital volume data. The rendered volume image reveals realistic 3D structures and interactions between the different lesions of the human breast. The volume can be observed at any orientation by using one of three different rendering methods. A graphic

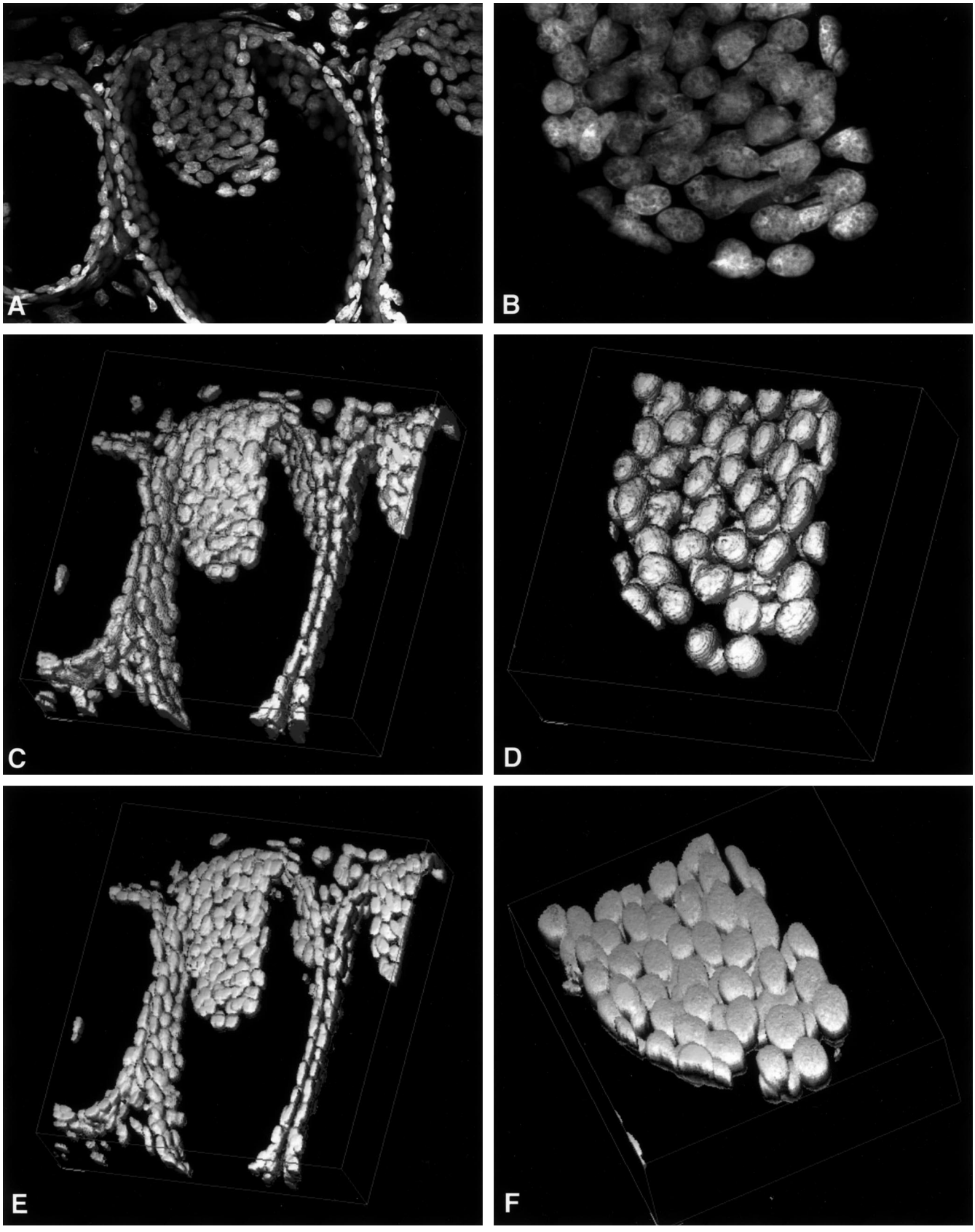

Fig. 3 **A** Digital image projection of Z-series of 40 optical sections (60× objective, 0.6-µm Z-step interval) taken by CLSM from a 30-µm-thick section of intraductal papillary hyperplasia of the human breast. **B** Higher magnification reconstruction of 28 optical sections showing cells within duct (60× objective, 0.3-µm Z-step interval, 2.6× electronic zoom). The nuclear chromatin texture and the morphologic features are similar to those shown for simple hyperplasia in Fig. 2A, B. **C** 3D surface display and **E** volume render of the duct shown in **A**. **D** 3D surface display and **F** volume render of higher magnification image of duct shown in **B**. Rotation angle was –21° on both the *x* and the *y* axes, and –7° on the *z* axis (**C–E**), and –36° on the *x* axis, 6° on the *y* axis, and 23° on the *z* axis (**F**)

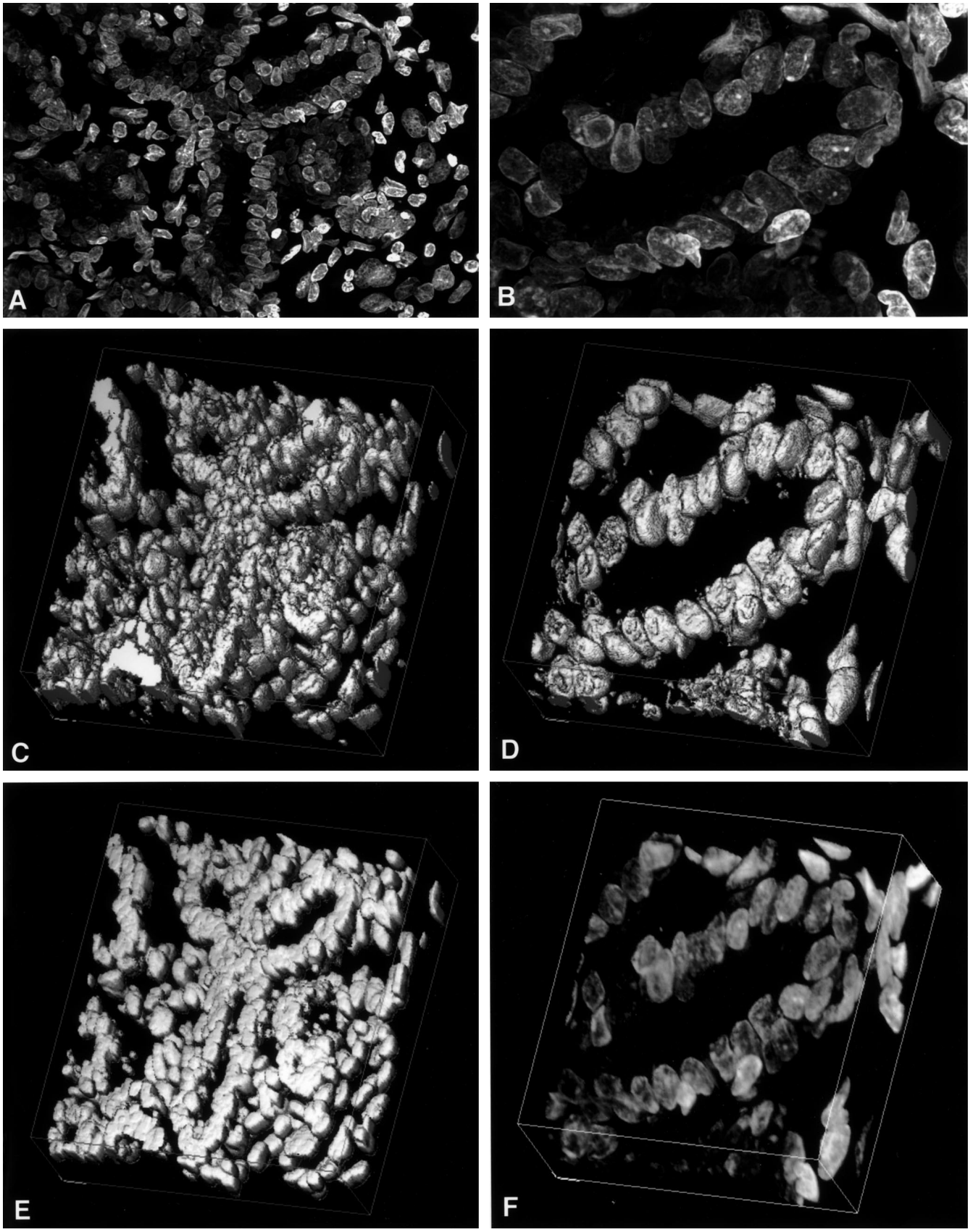

Fig. 4 **A** Digital image projection of Z-series of 49 optical sections (60× objective, 0.6-µm Z-step interval) taken by CLSM from a 30-µm-thick section of a fibroadenoma of the breast. **B** Higher magnification digital image projection of Z-series of 62 optical sections from the same area as in **A** (60× objective, 0.3-µm Z-step interval, 2.6× electronic zoom). Much clearer, in-focus images show tumor cell nuclei with similar size and shape. Other morphologic features are also similar to those displayed by hyperplasias, as shown in Figs. 2, 3. The interstitial fibroblasts are prominent. **C** Shaded surface display and **E** volume render of the same field as in **A**. **D** Shaded surface display and **F** volume render of of the same field as in **B**. Higher power 3D view of shaded surface display shows slightly rough nuclear surface. 3D view of volume render of the same field shown in **B**, rendered with the mode of Sum Voxels **F**, reveals the fine chromatin texture of tumor cell nuclei. One to two small nucleoli could be seen in some nuclei. Rotation angle was the same for C–F (–21° on the *x* and *y* axes, –7° on the *z* axis)

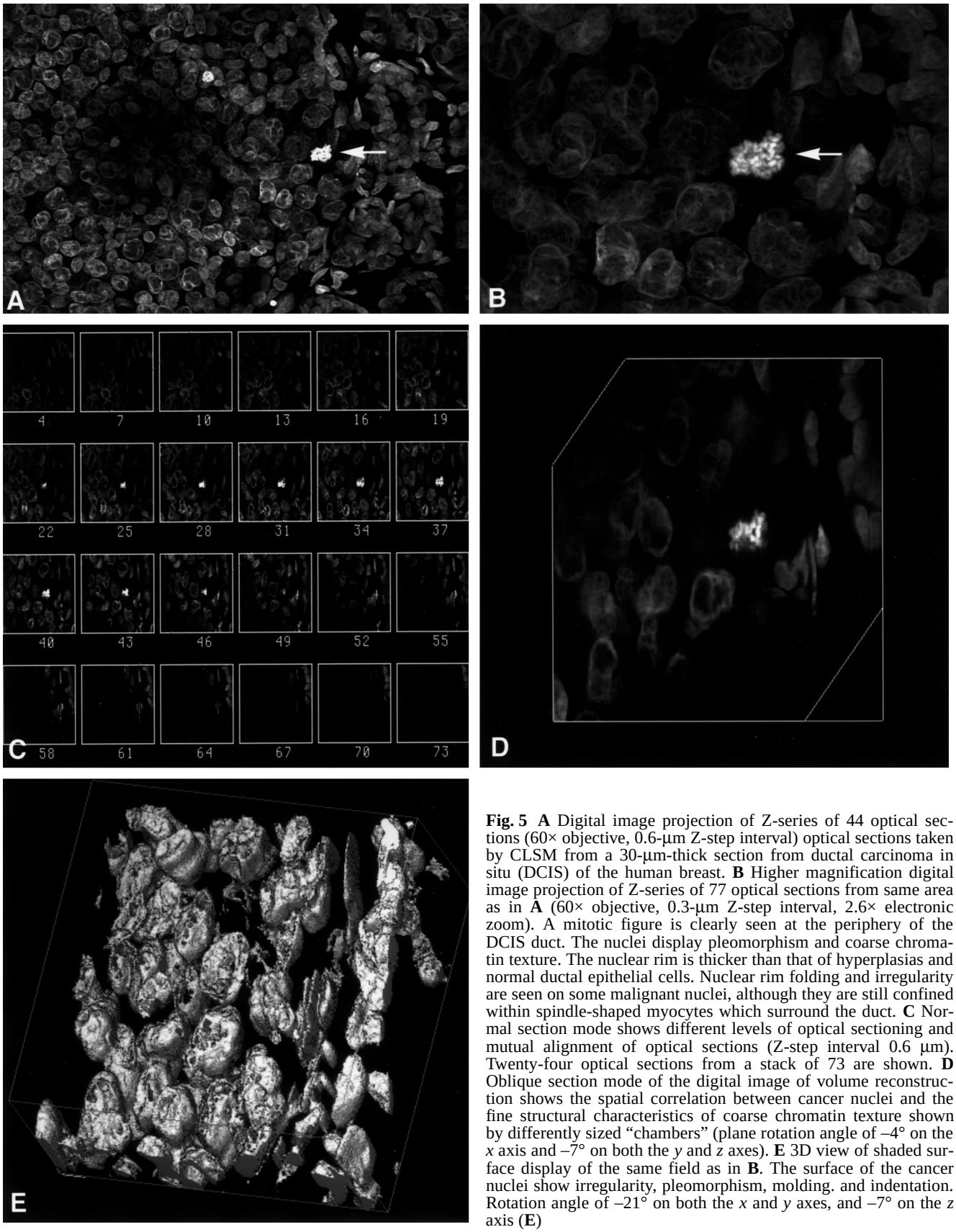

Fig. 5 **A** Digital image projection of Z-series of 44 optical sections (60× objective, 0.6-μm Z-step interval) optical sections taken by CLSM from a 30-μm-thick section from ductal carcinoma in situ (DCIS) of the human breast. **B** Higher magnification digital image projection of Z-series of 77 optical sections from same area as in **A** (60× objective, 0.3-μm Z-step interval, 2.6× electronic zoom). A mitotic figure is clearly seen at the periphery of the DCIS duct. The nuclei display pleomorphism and coarse chromatin texture. The nuclear rim is thicker than that of hyperplasias and normal ductal epithelial cells. Nuclear rim folding and irregularity are seen on some malignant nuclei, although they are still confined within spindle-shaped myocytes which surround the duct. **C** Normal section mode shows different levels of optical sectioning and mutual alignment of optical sections (Z-step interval 0.6 μm). Twenty-four optical sections from a stack of 73 are shown. **D** Oblique section mode of the digital image of volume reconstruction shows the spatial correlation between cancer nuclei and the fine structural characteristics of coarse chromatin texture shown by differently sized "chambers" (plane rotation angle of –4° on the *x* axis and –7° on both the *y* and *z* axes). **E** 3D view of shaded surface display of the same field as in **B**. The surface of the cancer nuclei show irregularity, pleomorphism, molding. and indentation. Rotation angle of –21° on both the *x* and *y* axes, and –7° on the *z* axis (**E**)

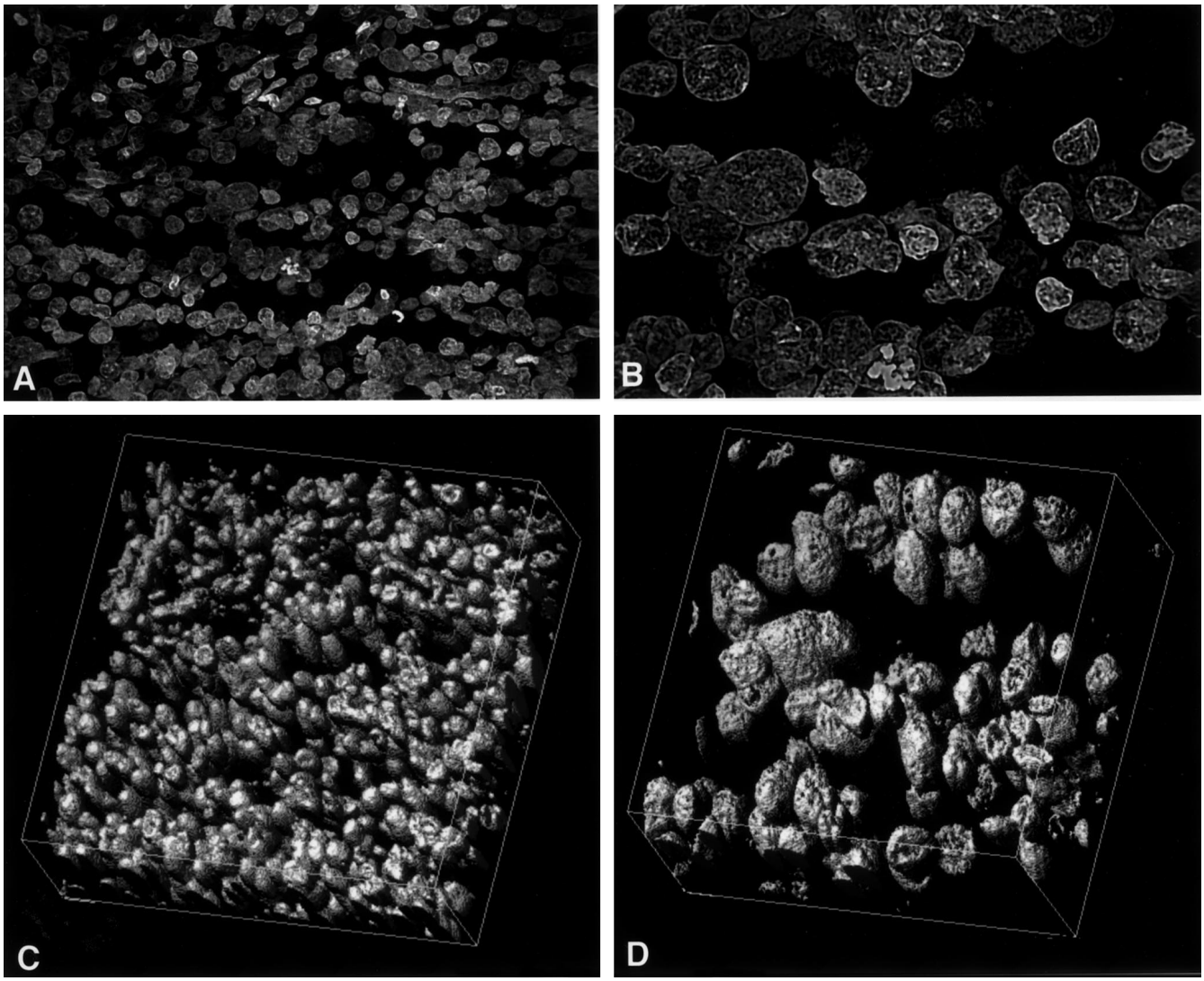

Fig. 6 **A** Digital image projections of Z-series of 48 optical sections taken by CLSM from a 30-μm-thick section of ductal invasive carcinoma of the human breast (60× objective, 0.6-μm Z-step interval). **B** Higher magnification digital image projection of Z-series of 71 optical sections of the same area as in **A** (60× objective, 0.3-μm Z-step interval, 2.6× electronic zoom). No ductal structure or myocytes are seen. The nuclei are enlarged and pleomorphic in shape. Coarse and hyperchromatic chromatin, as well as increased number and size are seen. **C** 3D view of the invasive ductal carcinoma shown in **A**, rendered with shaded surface display mode. The cancer nuclei are in a disordered arrangement. **D** Higher power 3D view of the same field shown in **B**. Increased size, pleomorphic shape, and molding of the nuclei are apparent with the shaded surface display. The spatial correlation is irregular and chaotic. Rotation angle was –21° on the *x* and *y* axes and –7° on the *z* axis

overlay throughout the 3D display features is presented that shows an outline of the volume being used. This volume reference cube is presented to help the investigator understand the orientation of the volume in space. A constant volume image scale of 65% was fixed for all the 3D volume image analysis, corresponding to the scale chosen for SSD rendering. In volume rendering, sequences of optical slices can be visualized as a 3D image, mimicking the tissue presentation of the breast sections. Prior to initiating the volume rendering procedure, an opacity value (including intensity) was assigned to the area of interest. The intensity value selected for our data rendering ranged from a low of 10–80 voxels to a high value of 110–255 voxels, depending on the original intensity condition of the digital image data. Once a satisfactory way of viewing a given image data volume has been determined, volume render can automatically generate an animation sequence which can be viewed later in the animation option. The volume render modes applied for our data sets were “First” and “Sum” voxel modes. In the former, each ray continues further and further into the volume until it strikes a voxel whose intensity is in the specified included range. The submode “Raw Data” was selected for displaying the raw intensity value of the first voxel encountered within the specified threshold include range. This rendering mode provides good qualitative information about the 3D structure of the lesion being studied (Figs. 1D, 2C, D, 3E, F, 4E). The other rendering mode we used was the “Sum” voxel mode. In this mode, all voxels which are within the in-

cluded range are summed and then divided by the number of voxels that have been summed; that is, the mean value of the voxels along each ray is computed and displayed. This creates an effect much like traditional X-ray images, which is advantageous for analyzing the fine structure of chromatin patterns inside the nucleus (Fig. 4F). Prior to applying this mode, the gamma value should be carefully adjusted to obtain satisfactory contrast and brightness of the displayed 3D image. For most of our image data, the gamma values we selected ranged from 1.50 to 1.80, depending on the original 3D digital image data. By setting the gamma value >1, thus making the overall volume object more transparent, fine structural detail reflected by the different fluorescent intensities was revealed. 3D reconstructions rendered via volume render mode are shown in Fig. 1D (normal mammary duct), Fig. 2C, D (hyperplastic mammary duct), Fig. 3E, F (intraductal papillary hyperplasia), and Fig. 4E, F (fibroadenoma of the breast).

3D morphologic features of benign lesions of the human breast

The clearly benign lesions of the breast (simple ductal hyperplasia and intraductal papillary hyperplasia) revealed similar 3D morphologic features to those demonstrated in the normal mammary duct, including: (1) smooth nuclear surface and homogeneous chromatin fluorescence intensity; (2) hyperplastic cell nuclei showing similar shape and volume; and (3) clear-cut margin of basement membrane defined by spindle-shaped myocytes of the ductal outer layer (Figs. 1C, D, 2C, D, 3C–F, 4C–F).

3D morphologic features of malignancies of the human breast

In contrast, carcinomas (ductal carcinoma in situ, ductal invasive, and lymph node metastatic carcinoma) displayed remarkably different features in 3D morphology, including: (1) indented, molding, and irregular nuclear surface;(2) marked pleomorphism (irregular, angulated, and indented shape of nuclear volume); (3) irregular and coarse chromatin texture; (4) chaotic arrangement of tumor cell nuclei; and (5) absence of myocytes, indicating no clear margin at the site of infiltration of cancer cells. Figures 5E and Fig. 6C, D are representative examples from a ductal carcinoma in situ and a ductal invasive carcinoma of the breast, respectively. Furthermore, a specific, particularly interesting nucleus and a subtle chromatin texture, as well as their mutual correlation, could be examined by the options of Normal Sections and Oblique Sections provided by the microVoxel program, as demonstrated in Fig. 5C, D.

Discussion

Pathologists have to use their imagination to capture a rough 3D image when observing an object under a conventional light microscope, since no atlas of 3D micrographs is available in diagnostic textbooks. The problems of the light microscope are similar to those encountered when one tries to see detail in thick histologic sections. In these 3D objects, axial resolution is poor and the inherent blurred image often lacks diagnostic detail (Boon et al. 1993). Confocal imaging and 3D digital image processing techniques provide high efficacy for 3D visualization of biologic and pathologic materials. The theoretically (and practically) improved visibility of optical sections and improved resolution (Michael and Hester 1995; Lucas et al. 1996; Figs. 1–6) brings pathologists from traditional 2D visualization of routinely processed specimens to a novel 3D realm.

In the present paper, the 3D reconstruction based on thinner (0.3–0.6 μm) optical sections with much clearer images of routine formalin-fixed, paraffin-embedded specimens of various entities of human breast have demonstrated 3D contour of representative lesions of benign and malignant epithelial lesions and the spatial relationship of nuclei, as well as the subtle structure of chromatin texture inside nuclei in great detail with truly 3D images (Figs. 1, 2C, D, 3C–F, 4C–F, 5C–E, 6C, D). Moreover, additional diagnostic information could be obtained by examining different planes of serial optical sections. For instance, nuclei with diagnostic features of malignancy were hidden in a lesion which looked benign or uncertain with conventional wide-field light microscopy (S. Liu et al., unpublished data). Thus, confocal imaging, together with 3D reconstruction techniques is proving to be a powerful tool in surgical pathology, especially in discriminating problematic lesions from biologically malignant ones, enabling earlier detection of cancer (preclinically manifested stage) (Rigaut et al. 1991; Smith et al. 1991; Sasano et al. 1993; Boon et al. 1993, 1994, 1995; Tekola et al. 1994a; King et al. 1995; Michael and Hester 1995; Shotton 1995).

In recent years, CLSM together with 3D reconstruction has been applied in numerous cell biological applications (Boyde 1985; van der Voort et al. 1985, 1989; Carlsson et al. 1989; Shotton 1989, 1995; Shuman et al. 1989; König et al. 1991; Beltrame et al. 1992; Cox 1993; Matsumoto and Kramer 1994), leading to a better understanding of cellular processes and structures. A few recent publications using CLSM and 3D reconstruction techniques have provided excellent examples for demonstrating the usefulness of these techniques in the clinical diagnosis of cytologic materials (Boon et al. 1993, 1994, 1995). By examining the thick fragments of cervical smears and breast aspirates using non-invasive optical sectioning, the irregular chromatin distribution and hidden mitotic figures were revealed in otherwise undiagnosticable specimens. Furthermore, utilizing 3D reconstruction techniques, the epithelial architecture of cancer and the abnormal spatial relationship of cancer

cell nuclei have been recognized (Boon et al. 1993). Other investigators have combined CLSM and 3D reconstruction to perform powerful quantitative analyses on nuclear structures from surgical pathology biopsy specimens. Zhu and co-workers (Zhu et al. 1994) calculated the volume and shape of cell nuclei in a 50-μm-thick section from a normal skin biopsy. Beil and co-workers (Beil et al. 1995) analyzed 3D chromatin texture in an elegant study of a large series of sections from prostatic lesions. They introduced 15 texture features used for lesion classification purposes, and achieved a classification accuracy of 91.7% for a training set of nuclei and 93.3% for a test set of nuclei from differentiating prostatic hyperplasia, dysplasia, and carcinoma. Although these quantitative methods are presently quite time consuming, they may secure a future role in the diagnostic pathology laboratory through automation and increased computer speed.

As indicated earlier, this paper emphasized the practical feasibility of CLSM and 3D reconstruction from routine surgical histopathologic materials and demonstrated the 3D morphologic features of entities from normal, clearly benign to biologically malignant lesions. To obtain desirable quality 3D images from formalin-fixed, paraffin-embedded specimens, YOYO-1 iodide, a highly specific and sensitive (picogram sensitivity) (Tekola et al. 1994b) DNA probe was utilized. Intense and homogeneous fluorescence was obtained by performing the YOYO-1 iodide incubation for 1 h with agitation in the dark. To reveal subtle details of nuclear structure, RNA was removed by RNase predigestion, since YOYO-1 iodide also stains nuclear RNA (Tekola et al. 1994b). To minimize the fluorescence bleaching, low laser intensity was applied during the optical sectioning. This ensured homogeneity of the fluorescence intensity of the whole stack of serial optical sections, providing good quality 2D and 3D digital images with subtleties of nuclear morphology revealed. To create realistic 3D digital images obtained from the paraffin-embedded tissues, various techniques of image processing and enhancement were essential, including adequate thresholding and correction of anisotropic voxels resulting from the artifact of flattening by the coverslip. Fluorescence intensity varies amongst specimens, and therefore values of different image processing parameters need to be predefined properly by the investigator before 3D volume rendering is performed. Otherwise, the resulting images are unsatisfactory, lacking actual expected architecture and containing random background noise.

CSLM combines the most advanced and important three elements of our era: the microscope, the laser, and the computer. Taking advantage of these attributes, we have successfully reconstructed 3D volume images from routine formalin-fixed, paraffin- embedded specimens of the human breast. The 3D morphologic features of benign lesions of the breast, including normal mammary tissue, were demonstrated, and constitute 3D diagnostic criteria for differentiating malignant from benign lesions. All the benign lesions showed similar cytologic characteristics to those revealed in normal mammary duct epithelium in 3D morphologic images, including a similar size and shape of round or ovoid nuclei, similar and homogeneous intensity of nuclear DNA fluorescence, and a smooth and regular nuclear rim. In comparison with those 3D morphologic features revealed in the benign tissues, malignant cell nuclei were stacked, chaotic in spatial arrangement, irregular in shape and displayed various sizes. Nuclear rims appeared rough, angulated or indented, manifested by coarse and irregularly distributed chromatin patterns.

CLSM bridges the large gap between light and electron microscopy, with the advantage that the technique is non-invasive and can be used on archival paraffin blocks. For the histopathologist this means that the observations are highly relevant for diagnostic work. We anticipate that, in the future, pathologists may utilize these new techniques to make more precise diagnostic decisions by visualizing the specimen in a realistic 3D mode, and at any desired thin optical sectioning level, which is more informative than the traditional light microscopic image.

Acknowledgements This work has been supported in part by a Mini-grant from the Cell Imaging Facility of the College of Medicine, University of Vermont to S.L. (SCH 003). The authors wish to thank Susan Edgerton and Marilyn Wadsworth for their excellent technical assistance, and Professor Ann Thor for her advice on study design. We also gratefully thank Mr. Norbert Wey (Department of Pathology, University of Zurich, Switzerland) for his time and effort towards the final preparation of the digital images, improving the quality of this manuscript.

References

Beil M, Irinopoulou T, Vassy J, Rigaut JP (1995) Chromatin texture analysis in three-dimensional images from confocal scanning laser microscopy. Anal Quant Cytol Histol 17:323–331

Beltrame FP, Ramoino M, Fato MUD, Corrado G, Marcenaro, Franceschi TC (1992) Three-dimensional reconstruction of *Paramecium primaurelia* oral apparatus through confocal laser scanning optical microscopy. Micron 23:403–412

Boon ME, Kok LP, Sutedja G, Dutrieux RP (1993) Confocal sectioning of thick, otherwise undiagnosable cell groupings in cervical smears. Acta Cytol 37:40–48

Boon ME, Schut JJ, Benita EM, Kok LP (1994) Confocal optical sectioning and three-dimensional reconstruction of carcinoma fragments in pap smears using sophisticated image data processing. Diagn Cytopathol 10:268–275

Boon ME, Schut JJ, Suurmeijer AJH, Benita EM, PKH Hut, Kok LP (1995) Confocal microscopy of false-negative breast aspirates. Diagn Cytopathol 12:42–50

Boyde A (1985) Stereoscopic images in confocal (tandem scanning) microscopy. Science 230:1270–1272

Brakenhoff GJ, Voort HTM van der, Spronsen EA van, Linnemans WAM, Nanninga N (1985) Three-dimensional chromatin distribution in neuroblastoma nuclei shown by confocal scanning laser microscopy. Nature 317:748–749

Carlsson K, Wallen P, Brodin L (1989) Three-dimensional imaging of neurons by confocal fluorescence microscopy. J Microsc 155:15–26

Chen H, Swedlow JR, Grote M, Sedat JW, Agard DA (1995) The collection, processing, and display of digital three-dimensional images of biological specimens. In: Pawley JB (ed) Handbook of biological confocal microscopy. Plenum Press, New York, pp 197–210

Cox G (1993) Trends in confocal microscopy. Micron 24:237–247
King JAC, Hester RB, Titford ME, Michael C (1995) Psammoma bodies: confocal microscopy with 3D reconstruction of two-color fluorescence on paraffin-embedded sections and cytology smears. Cell Vision 2:420–424
König D, Carvajal-Gonzalez S, Downs AM, Vassy J, Rigault JP (1991) Modelling and analysis of 3D arrangements of particles by point processes with examples of application to biological data obtained by confocal scanning light microscopy. J Microsc 161:405–433
Lucas L, Gilbert N, Ploton D, Bonnet N (1996) Visualization of volume data in confocal microscopy: comparison and improvements of volume rendering methods. J Microsc 181: 238–252
Matsumoto B, Kramer T (1994) Theory and applications of confocal microscopy. Cell Vision 1:190–198
Michael C, Hester RB (1995) Editorial comments: confocal microscopy: a new horizon for cytology. Diagn Pathol 12:49–50
Rigaut JP, Vassy J, Herlin P, Duigou F, Masson E, Briane D, Foucrier J, Carvajal-Gonzalez S, Downs AM, Mandard A-M (1991) Three-dimensional DNA image cytometry by confocal scanning laser microscopy in thick tissue blocks. Cytometry 12:511–524
Sasano H, Date F, Itakura Y, Goukon Y, Nishihara T, Nagura H (1993) Confocal laser scanning microscopy in cytopathology. Mod Pathol 6:625–629
Shotton DM (1989) Confocal scanning optical microscopy and its application for biological specimens. J Cell Sci 94:175–206
Shotton DM (1995) Electronic light microscopy: present capabilities and future prospects. Histochem Cell Biol 104:97–137
Shuman H, Murray JM, DiLullo C (1989) Confocal microscopy: an overview. Biotechniques 7:154–163
Smith GJ, Bagnell CR, Bakewell WE, Black KA, Bouldin TW, Earnhardt TS, Hook GER, Pryzwansky KB (1991) Application of confocal scanning laser microscopy in experimental pathology. J Electron Microsc Tech 18:38–49
Tekola P, Zhu Q, Baak JPA (1994a) Confocal laser microscopy and image processing for three-dimensional microscopy: technical principles and an application to breast cancer. Hum Pathol 25:12–21
Tekola P, Baak JPA, Belien JAM, Brugghe J (1994b) Highly sensitive, specific, and stable new fluorescent DNA stains for confocal laser microscopy and image processing of normal paraffin sections. Cytometry 17:191–195
Voort HTM van der, Brakenhoff GJ, Valkenburg JAC, Nanninga N (1985) Design and use of a computer controlled confocal microscope for biological applications. Scanning 7:66–78
Voort HTM van der, Brakenhoff GJ, Baarslag MW (1989) Three-dimensional visualization methods for confocal microscopy. J Microsc 153:123–132
Zhu Q, Tekola P, Baak JPA, Belien JAM (1994) Measurement by confocal laser scanning microscopy of the volume of epidermal nuclei in thick skin sections. Anal Quant Cytol Histol 16:145–152